Polymer(Korea), Vol. 40, No. 2, pp. 167-174 (2016)
http://dx.doi.org/10.7317/pk.2016.40.2.167

ISSN 0379-153X(Print)
ISSN 2234-8077(Online)

용매 Intercalation에 의한 Poly(lactic acid)/산화아연-Pillared 유기 사포나이트 나노복합재료의 성능과 구조분석

Weijun Zhen†, Shengzhen Bian*, Jinlu Sun, and Xi Xi

Key Laboratory of Oil and Gas Fine Chemicals, Ministry of Education and Xinjiang Uygur Region, Xinjiang University
*Xinjiang Institute of Light Industry Technology

(2015년 7월 31일 접수, 2015년 9월 30일 수정, 2015년 11월 2일 채택)

Performance and Structure Characterization of Poly(lactic acid)/Zinc Oxide Pillared Organic Saponite Nanocomposites by Solution Intercalation

Weijun Zhen†, Shengzhen Bian*, Jinlu Sun, and Xi Xi

Key Laboratory of Oil and Gas Fine Chemicals, Ministry of Education and Xinjiang Uygur Region, Xinjiang University, Urumqi 830046, China
**Xinjiang Institute of Light Industry Technology, Urumqi 830021, China*

(Received July 31, 2015; Revised September 30, 2015; Accepted November 2, 2015)

Abstract: Zinc oxide (ZnO) pillared organic saponite was synthesized with cetyltrimethylammonium bromide (CTAB) via a microwave hydrolysis method. Moreover, poly(lactic acid) (PLA)/ZnO pillared organic saponite nanocomposites were prepared by solution intercalation. The microstructure analysis suggested that ZnO pillared organic saponite appeared at an exfoliated or partially intercalated nanometer layer, which dispersed homogeneously in PLA matrix. The experimental results showed that ZnO pillared organic saponite improved the mechanical properties and thermal stabilities of PLA/ZnO pillared organic saponite nanocomposites. Differential scanning calorimetry (DSC) results demonstrated that the ZnO pillared organic saponite eliminated the cold crystallization process, decreased the crystal size and obviously promoted the crystallinity of PLA, which was in accordance with XRD analysis results. At the same time, the properties of UV absorbance and antibacterial properties of nano ZnO were introduced into PLA.

Keywords: poly(lactic acid), ZnO pillared organic saponite, nanocomposites, performance, structure.

Introduction

Poly(lactic acid) (PLA) is a biodegradable thermoplastic polymer, derived from renewable natural resources such as cornstarch, sugarcane and attracted much attention due to their unique properties.[1] PLA has low toxicity and good barrier properties, which served this polymer as a potential candidate into wide range of industrial applications, such as food packaging, textile industries and many other engineering fields.[2,3] On the other hand, the main disadvantage of PLA is its low crystallinity, which makes it highly brittle, consequently lowering its mechanical strength.[4-6] In order to overcome this problem, researchers synthesized polymer/clay nanocomposites, which can be a potential candidate because of their excellent mechanical properties, thermal stability, gas barrier, and optical properties with low clay content.[7,8] Some studies reported[9-11] that a small amount of nanofillers improved the comprehensive performance of PLA materials.

Saponite is a specific layered silicate mineral, which has trioctahedron structure with excellent properties.[12] On the other hand, zinc oxide (ZnO) has the potential for use in a wide range of applications, such as magnetic, optical, electrical and so on.[13-15] In the previous work,[16] ZnO pillared saponite was prepared via a microwave hydrolysis method to provide PLA materials the properties of ZnO and to improve their crystalline properties. In order to enhance the interfacial compatibility of ZnO pillared saponite with PLA matrix, cetyltrimethyl ammonium bromide (CTAB) was used to organically modify ZnO pillared saponite.[6] Moreover, PLA/ZnO pillared organic saponite nanocomposites were prepared by melting processing. The

†To whom correspondence should be addressed.
E-mail: zhenweijun6900@163.com

microstructure analysis and mechanical properties of thermoplastic PLA/ZnO pillared organic saponite nanocomposites were studied, which showed that ZnO pillared organic saponite had a good interfacial compatibility and heterogeneous nucleation effect in PLA matrix, and also played an active role in improving in mechanical properties of PLA. In the present work, in order to expand the application fields of PLA materials, the functional PLA based nanocomposites were prepared by solution intercalation. The UV absorption properties, antibacterial properties and structure characterization of PLA/ZnO pillared organic saponite nanocomposites were investigated, respectively.

Experimental

Materials. PLA (L-form, injection grade, M_v=80000 g/mol), was purchased from Shenzhen Guanghuaweiye Industrial Co., China. Saponite powder (mean grain size was about 60-70 μm) was purchased from Xinjiang Tuogema Colloid Co., China. *N*, *N'*,*N''*-tricyclohexyl-1,3,5-benzenetricarboxylamide (TMC-328) (nucleating agent, industrial grade) was provided by Institute of Shanxi Chemical Industry, China. Analytically pure $ZnCl_2$ and cetyltrimethyl ammonium bromide (CTAB) were purchased from Tianjin Fuchen Chemical Reagent Factory, China. Analytically pure NaOH was provided by Tianjin Zhiyuan Chemical Reagent Factory, China. Analytically pure trichloromethane was provided by Tianjin North Star Zheng Fang Chemical Reagent Factory, China.

Bacillus subtilis and *E. coli* (*Escherichia coli*) were provided by The Agronomy Soil Microbiology Teaching and Research Section of Xinjiang Agricultural University.

Preparation of ZnO Pillared Organic Saponite. 10 wt% suspensions were made using 10 g of ZnO pillared saponite.[16] Then, 4.37 g of CTAB was dissolved in 300 mL of water and added into ZnO pillared saponite water suspensions to yield precipitates with a separating funnel under vigorous stirring in a water bath at 70 °C for 2 h. After filtration, the precipitates were washed with deionized water until no Br^- (examined by 0.1 mol/L $AgNO_3$) was detected and then dried to obtain ZnO pillared organic saponite.

Preparation of PLA/ZnO Pillared Organic Saponite Nanocomposites. 8.82 g of PLA was dissolved in 71 mL trichloromethane. After that, TMC-328 and sifted ZnO pillared organic saponite were added to the above solution, respectively, with vigorous stirring at room temperature. As soon as TMC-328 and ZnO pillared organic saponite were evenly dispersed in the solution, the solution was quickly poured into a glass culture dish in a fume cupboard. After trichloromethane was volatilized completely at normal temperature, PLA/ZnO pillared organic saponite nanocomposites were obtained as uniform thin films, each with a thickness of about 0.5 mm. Table 1 lists the details of mixing composition and name of all composites for the present studies.

Table 1. Mixing Compositions of PLA/ZnO Pillared Organic Saponite Nanocomposites

Compound code	Mixing composition		
	PLA (g)	TMC-328 (g)	ZnO pillared organic saponite
P0	8.82	-	-
PTZ0	8.82	0.026	-
PTZ3	8.82	0.026	0.026
PTZ5	8.82	0.026	0.044
PTZ7	8.82	0.026	0.062
PTZ9	8.82	0.026	0.079
PTZ15	8.82	0.026	0.132

*PTZ0 (3, 5, 7, 9, 15) indicated that the contents of ZnO pillared organic saponite were 0, 0.3, 0.5, 0.7, 0.9, 1.5% (w/w), respectively.

Tensile tests were carried out according to ASTM D 412-80 by Instron 4302, a universal testing machine at a crosshead speed of 5 mm/min. At least five measurements for each composite were performed.

Samples were Characterized by Using X-ray Diffraction (XRD). The experiment was carried out by using a Cu Kα source at λ = 0.1540 nm (50 kV, 35 mA) with Philips X'Pert X-diffractometer (Netherlands). Diffraction spectra were obtained between 2θ = 1.5° and 2θ = 60° with a scanning speed of 0.1 °/s.

The morphology of ZnO pillared organic saponite and the fracture surface of PLA/ZnO pillared organic saponite nanocomposites were examined by using scanning electron microscopy (SEM). Prior to SEM, samples were sputter-coated with gold to avoid the charging effect. SEM of ZnO pillared organic saponite was carried out using a FEI INSPECT F-SEM (Netherlands) operating at 20 kV. The PLA/ZnO pillared organic saponite nanocomposites were broken immediately after soaking in liquid nitrogen, and the fracture surfaces of the PLA/ZnO pillared organic saponite nanocomposites were analyzed by SEM. SEM was carried out using a HITACHI SU-8010 (Japan) operating at 5 kV.

Transmission electron microscopy (TEM) was used to analyze the morphology of ZnO pillared organic saponite. TEM

was carried out using a TECNAI G2-F20 at an accelerating voltage of 75 kV.

Thermal gravimetric (TG) analysis was performed on a TA-Q600 (USA). Samples of about 5-10 mg were placed in an open alumina crucible. Temperature was programmed from room temperature to 450 ºC with a heating rate of 10 ºC/min. The instrument was operated under a nitrogen purge (100 mL/min).

Differential scanning calorimetry (DSC) was conducted on a NETZSH 204 DSC differential scanning calorimeter. Samples of about 5-8 mg were performed by heating from room temperature to 250 ºC at a heating rate of 10 ºC/min under the nitrogen purge (40 mL/min).

UV absorption test was conducted by UV-2800 spectrophotometer with a range of wavelength (200-1000 nm). PLA/ZnO pillared organic saponite nanocomposites were cut into small slices of 2 cm in diameter.

The thin PLA based nanocomposites with 2 cm in diameter were put into the bacteria culture medium. Then, *Bacillus subtilis and Escherichia coli* were cultivated for 24 h. After that, the areas of bacteriostatic rings of PLA based nanocomposites were measured.

Results and Discussion

Morphological Analysis. Figures 1(a) and 1(b) show the SEM images of saponite and ZnO pillared organic saponite, respectively whereas the TEM images of saponite and ZnO pillard organic saponite are presented in Figures 1(c) and 1(d), respectively. The SEM image of saponite showed a uniformly layered structure with a smooth surface and no absorption of other particles (Figure 1(a)). Compared to Figure 1(a), the morphology of ZnO pillared organic saponite showed significant changes (Figure 1(b)). Figure 1(b) showed that some

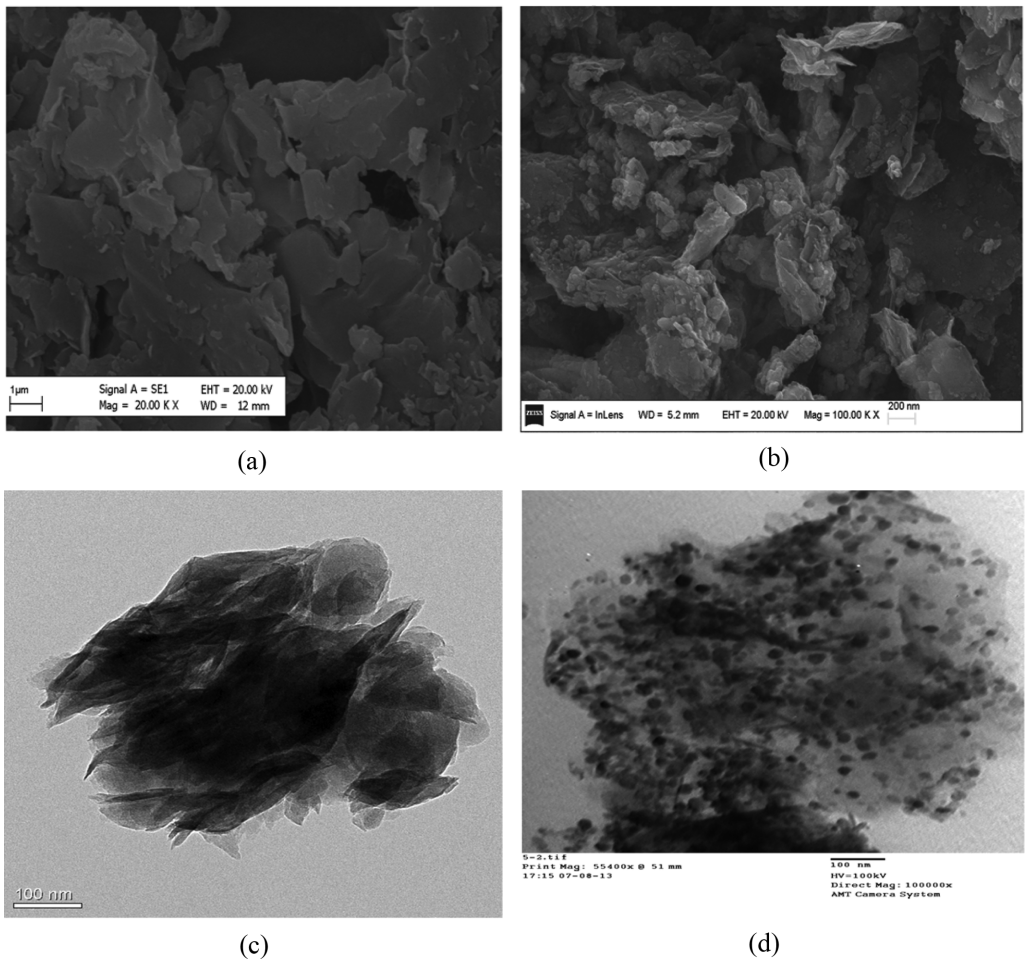

Figure 1. Morphological analysis of ZnO pillared organic saponite: (a) SEM images of saponite; (b) SEM images of ZnO pillared organic saponite; (c) TEM images of saponite; (d) TEM images of ZnO pillared organic saponite.

tiny nano ZnO particles were absorbed on the surface of saponite layer. On the other hand, it was found that a small part of nano ZnO was agglomerated due to the strong electrostatic adsorption effect.

In Figure 1(c),[17] the dark region shows the saponite phase, and the saponite layers appear aggregated. Compared to the pure saponite (Figure 1(c)), it was clearly observed from Figure 1(d) that the ZnO particles and saponite layers had dimensions ranging from 15 to 50 nm, indicating the existence of nano-sized ZnO pillared organic saponite. The partially exfoliated and intercalated structure of saponite can be clearly observed, and the d-spacing between the layers of saponite is enlarged. This could be well explained by combining these results with the XRD analysis of ZnO pillared organic saponite.

Mechanical Performance. Table 2 lists the mechanical properties of PLA/ZnO pillared organic saponite nanocomposites. It was shown that with the addition of TMC-328 and ZnO pillared organic saponite, the elongation at break (EL) decreased progressively. With the increase of TMC-328 and ZnO pillared organic saponite content, the reduction of the ductility in the PLA/ZnO pillared organic saponite nanocomposites might be related to the strong interfacial interaction between the fillers and PLA, which restrained the mobility and the growth of PLA molecular chains in PLA matrix and resulted in the reduction of toughness of the PLA based nanocomposites. It was clear from Table 2 that with the addition of TMC-328, the tensile stress (TS) of the PLA based nanocomposites increased significantly compared to the neat PLA. This phenomenon could be attributed to the excellent heterogeneous nucleation effect of TMC-328, which improved the crystallization of PLA.[18,19] The TS increased rapidly with an increase in the addition of ZnO pillared organic saponite from 0 to 0.5 phr, and the maximum TS of PTZ5 reached at 43.94 MPa, which was 163% higher than that of P0 (16.73 MPa). It was shown that the optimum addition of ZnO pillared organic saponite was 0.5 phr. The reason was a small amount of ZnO pillared organic saponite could be evenly dispersed into the PLA matrix at exfoliated nanometer layer, which increased the contact area and interaction between ZnO pillared organic saponite layers and PLA molecular chains.[20] Moreover, ZnO pillared organic saponite surface absorbed many organic groups, which could enhance the interfacial compatibility of ZnO pillared organic saponite in PLA matrix. Therefore, ZnO pillared organic saponite performed a good heterogeneous nucleation effect, which improved the crystallinity of PLA. This resulted in the reinforcement of mechanical performance of PLA based nanocomposites. On the other hand, when the addition of ZnO pillared organic saponite was more than 0.5 phr, the TS of PLA based nanocomposites (PTZ7, PTZ9, PTZ15) decreased gradually. The main reason was that ZnO pillared organic saponite aggregated in PLA matrix, which impeded the motion and development of PLA molecular chain and formed stress points. Therefore, it would be easy to break under the effect of outside force.[12,21,22]

Table 2. Mechanical Properties of PLA/ZnO Pillared Organic Saponite Nanocomposites

Samples	Maximum tensile stress (MPa)	Elongation at break (%)
P0	16.73±0.77	66.73±3.34
PTZ0	32.54±2.04	26.04±1.22
PTZ3	41.24±2.16	22.66±1.13
PTZ5	43.94±2.20	20.80±1.04
PTZ7	42.40±2.12	18.48±0.92
PTZ9	40.63±2.02	17.92±0.90
PTZ15	39.47±1.99	16.58±0.83

Fracture Surface Analysis. The fracture characteristics of PLA based nanocomposites were obtained from SEM images. Figure 2 showed the SEM images of tensile fractured surfaces of P0 (neat PLA), PTZ0 and PTZ5. Figure 2(a) showed a relatively smoother and complete fractured surface, indicative of a brittle fracture. However, the surface roughness of fractured area of PTZ0 (Figure 2(b)) was clearly increased compared to P0. And some tiny filaments were adhered to the rough phase interface of PTZ0, which was the characteristic of toughness fracture. This was due to the effect of TMC328 since TMC328 was added as a nucleating agent to increase the toughness of the PLA. Furthermore, Figure 2(c) (PTZ5) showed a much rougher phase interface with numerous filaments and toughness cavities, which proved to be a typical toughness fracture and explained the improvement in toughness on the introduction of ZnO pillared organic saponite.

XRD Analysis. Figure 3(a) shows the X-ray diffraction patterns of ZnO pillared organic saponite, ZnO pillared saponite and saponite. The first peak (001) in Figure 3(a) indicated the characteristic XRD reflections of saponite. The XRD patterns of ZnO pillared saponite indicated that the diffraction peak (001) was almost disappeared although the other peaks of ZnO (100), (002), (101), (102), (110) were distinct, which suggested that the layers of saponite were almost exfoliated into the nanometer scale layers by ZnO. Compared to the saponite, the

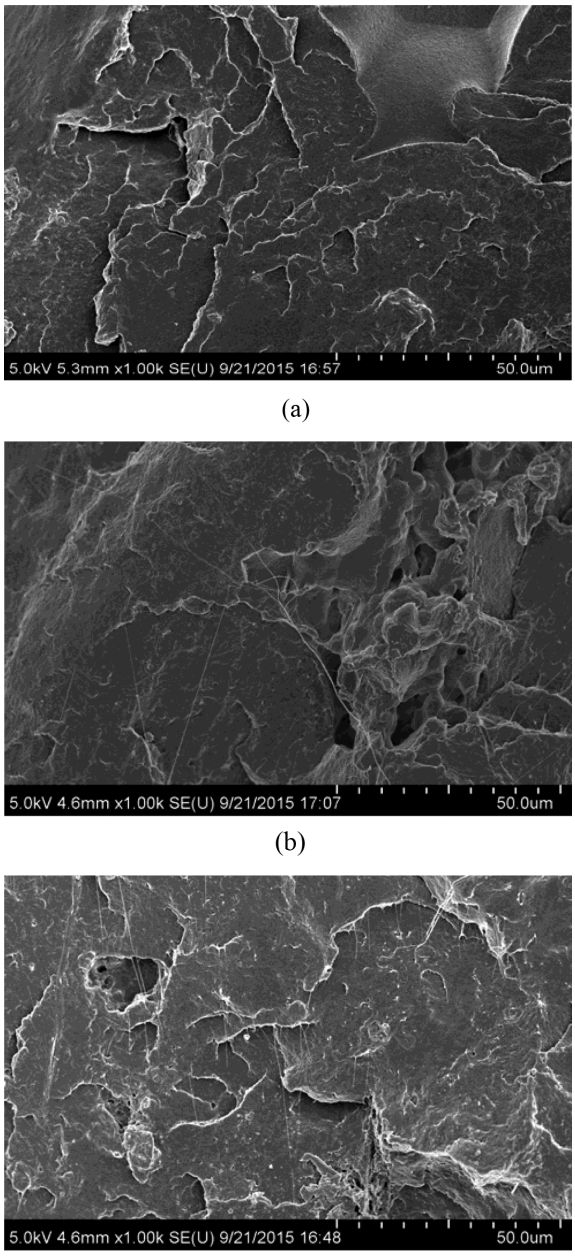

Figure 2. SEM images of fracture surfaces of P0, PTZ0 and PTZ5: (a) P0; (b) PTZ0; (c) PTZ5.

intensity of the first peak (001) of ZnO pillared organic saponite was very weak and the peak shifted towards the range of smaller angle, which showed that the ZnO pillared saponite was well modified by CTAB.

As shown in Figure 3(b), the neat PLA (P0) exhibited two peaks at about 2θ = 16.4° and 19.1° which prominently indicated a crystalline PLA matrix.[23] With the addition of TMC-328 and ZnO pillared organic saponite, the diffraction peaks of

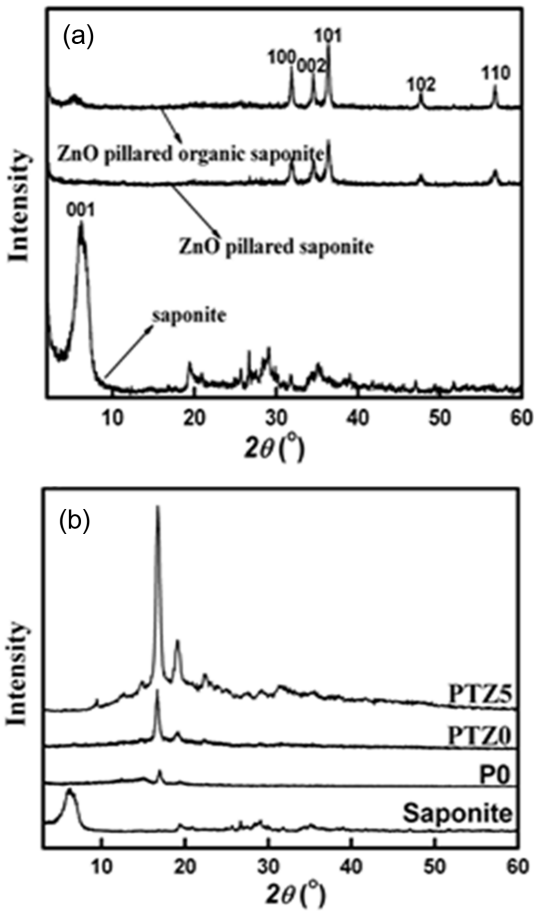

Figure 3. XRD patterns of ZnO pillared organic saponite, ZnO pillared saponite and saponite (a); PLA/ZnO pillared saponite nanocomposites (b).

PLA based nanocomposites became sharp, single and uniform compared to the P0, especially at 2θ = 16.4°. This phenomenon indicated that the crystallinity of PLA matrix was increased. Several factors could be responsible for this phenomenon. At first, ZnO pillared organic saponite attached many organic cations, which improved the interfacial compatibility with PLA matrix. This allowed the ZnO pillared organic saponite to disperse homogeneously in trichloromethane solution. Secondly, ZnO pillared organic saponite had good contact with the PLA molecular chains due to its excellent surface properties, which contributed to overcome the crystalline energy barrier of PLA matrix. At the same time, nanoscale ZnO pillared organic saponite increased the number of crystal nuclei and improved the heterogeneous nucleation effect. Finally, TMC-328 and ZnO pillared organic saponite had a synergistic effect, which enhanced the crystallization of PLA more effectively. From the patterns of PTZ, it was found that the characteristic peaks of

saponite were disappeared while comparing the patterns of saponite whereas the characteristic peaks of ZnO were observed at $2\theta = 30^{o}$-40^{o},[24] which proved that saponite was exfoliated into the nanometer scale layers by ZnO. On the other hand, trichloromethane broke the intermolecular hydrogen-bonding interactions in PLA, when PLA was dissolved in trichloromethane. This effect improved the mobility of the polymeric chains and influenced the ordering of PLA molecules, which was favorable for the crystallization during the volatilization process of trichloromethane.

DSC Analysis. Figure 4 shows DSC curves of the PLA based nanocomposites. The crystallization of the PLA based nanocomposites in Table 3 is given below:

$$X_c = \frac{\Delta H_m - \Delta H_c}{f \times \Delta H_m^0} \times 100\% \quad (1)$$

Where X_c is the degree of crystallinity of the PLA based nanocomposites, ΔH_c is the enthalpy of crystallization, ΔH_m is the enthalpy of fusion, f is the weight fraction of PLA in the composite and ΔH_m^0 is enthalpy of fusion of the purely crystalline form of PLA ($\Delta H_m^0 = 93.7$ J/g).[25]

Table 3 lists the details of experimental data. It was found that the glass transition temperature (T_g), and melting temperature (T_m) of PLA based nanocomposites shifted towards the lower temperature range while the cold crystallization disappeared after introducing TMC-328 and ZnO pillared organic saponite. The reason for this phenomenon could be that TMC-328 effectively enhanced the crystallization of PLA[18,26] and ZnO pillared organic saponite improved the interfacial compatibility between the inorganic and organic phases, which resulted in the reduction of activation energy for the crystallization of PLA. Therefore, the crystallization occurred more easily and the cold crystallization behavior of PLA was restrained. Table 3 showed that the crystallinity of PTZ5 was 48.1%, which increased by 109% than that of P0. This was consistent with the XRD analysis of PLA based nanocomposites. This result might be attributed to the heterogeneous

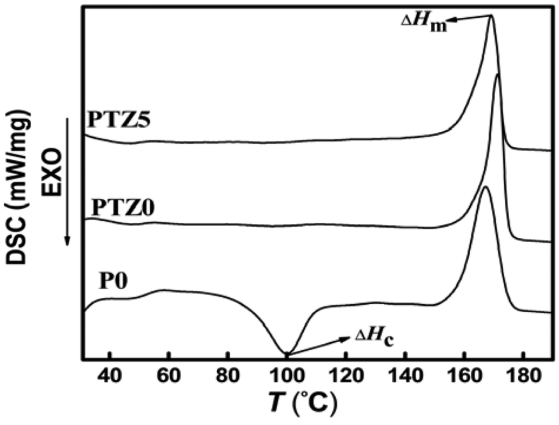

Figure 4. DSC curves of PLA based nanocomposites.

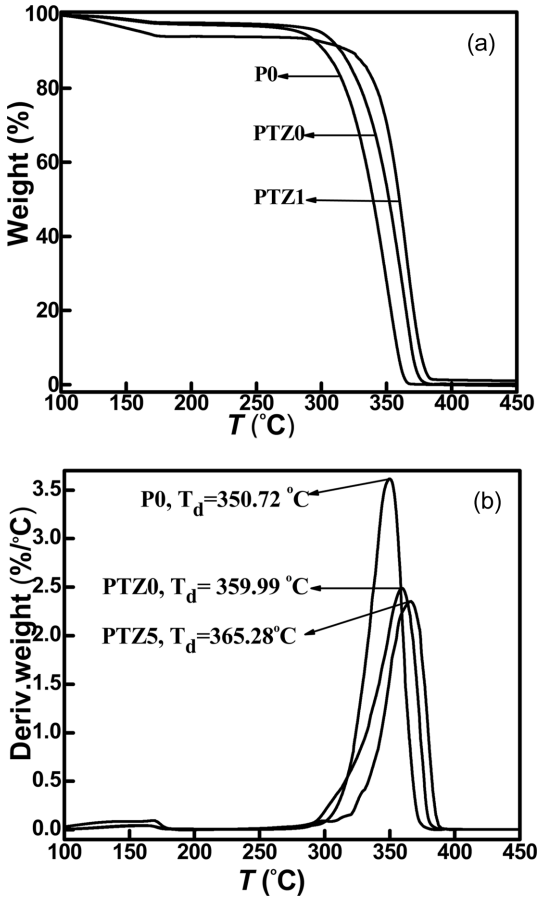

Figure 5. TG curves of PLA based nanocomposites.

Table 3. DSC Analysis of PLA and PLA/ZnO Pillared Organic Saponite Nanocomposites

Samples	T_o (°C)	T_∞ (°C)	T_g (°C)	T_m (°C)	ΔH_c (J·g^{-1})	ΔH_m (J·g^{-1})	X_c (%)
P0	158.2	174.8	55.7	166.9	-23.56	45.08	23.0
PTZ0	165.9	174.7	52.3	171.3	-	40.05	42.7
PTZ5	161.4	173.7	49.4	169.2	-	45.03	48.1

nucleation effect of TMC-328 and ZnO pillared organic saponite, which induced the crystallization of PLA synergistically. Moreover, the melting range of PLA/ZnO pillared organic saponite nanocomposites showed a good resemblance in terms of crystallinity compared to that of neat PLA, which indicated a good integrity of their single crystalline nature of PLA.

TG Analysis. Figure 5 shows the results of TG-DTG analysis of the PLA based nanocomposites. The experimental results indicated that after the addition of TMC-328, the thermal stability of PLA based nanocomposites was improved. When ZnO pillared organic saponite was introduced, the thermal decomposition temperature of PLA nanocomposites (PTZ5) increased by 14.56 ºC compared to that of neat PLA. The reason could be that ZnO pillared organic saponite impeded the thermal motion of PLA molecules in the matrix and therefore increased the energy barrier of the thermal decomposition of PLA. As a result, the thermal decomposition temperature of PLA materials was improved.

UV Absorption Properties. Figure 6 presents the ultraviolet absorption spectra of PLA based nanocomposites. The results showed that the ultraviolet absorption was obviously between 250-400 nm. Comparing to P0, the ultraviolet absorption was increased with the addition of ZnO pillared organic saponite. This phenomenon could be well explained on the fact that nano ZnO was incorporated into the saponite layers and eventually dispersed homogeneously into the PLA matrix. As an excellent ultraviolet screening material, nano ZnO could absorb the long and medium wavelength regions of light rays.[27] This effect hindered the UV rays through the PLA based nanocomposites and minimized its aging. Moreover, it was found that the ultraviolet absorption peaks of PLA based nanocomposites showed a blue shift between 340-400 nm. As a result, the ultraviolet excitation peak of PLA based nanocomposites required more energy,[15] which showed that the ultraviolet shielding of PLA based nanocomposites was improved on the increasing the addition of ZnO pillared organic saponite.

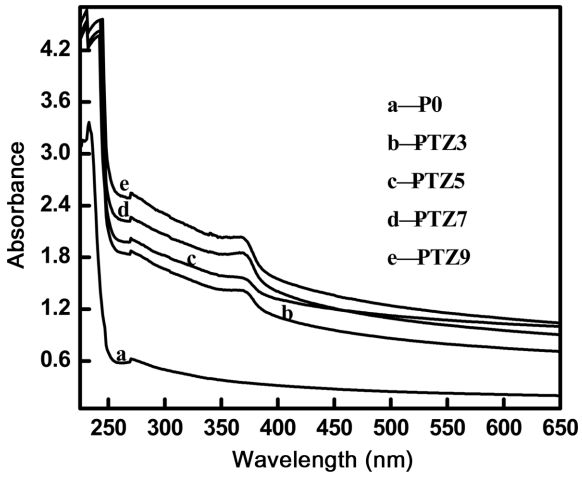

Figure 6. UV absorption curves of the PLA based nanocomposites.

Antibacterial Properties. Figures 7 and 8 represent the images of antibacterial effects of PLA based nanocomposites. Two types of bacteria e.g., *Bacillus subtilis* and *Escherihia coli* were chosen for this testing. It was found that the bacteriostatic ring appeared around the PLA based nanocomposites, which inhibited the growth of bacteria inside the ring. Table 4 shows

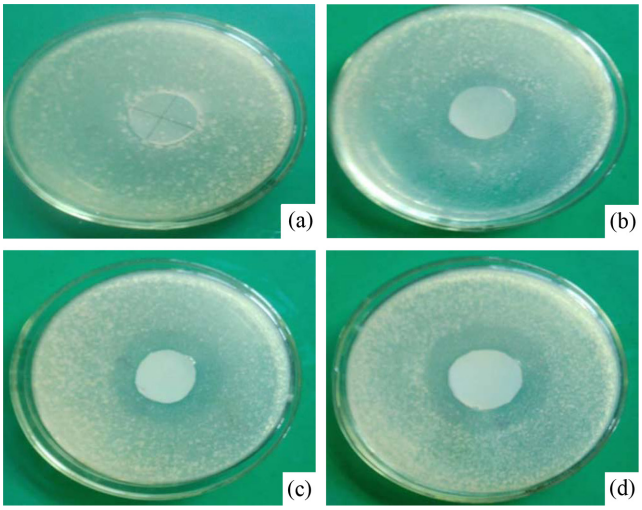

Figure 7. Antibacterial properties image of *Bacillus subtilis* of PLA based nanocomposites: (a) P0; (b) PTZ5; (c) PTZ9; (d) PTZ15.

Table 4. Antibacterial Areas of PLA Based Nanocomposites

Culture	*Bacillus subtilis*				*Escherichia coli*			
Compound code	P0	PTZ5	PTZ9	PTZ15	P0	PTZ5	PTZ9	PTZ15
PLA nanocomposites areas (cm^2)	3.80	3.82	3.78	3.81	3.71	3.69	3.67	3.72
Bacteriostatic areas (cm^2)	3.80	9.91	12.83	14.17	3.71	13.55	14.57	14.91
Bacteriostatic rings areas (cm^2)	0	6.09	9.01	10.36	0	9.86	10.90	11.19

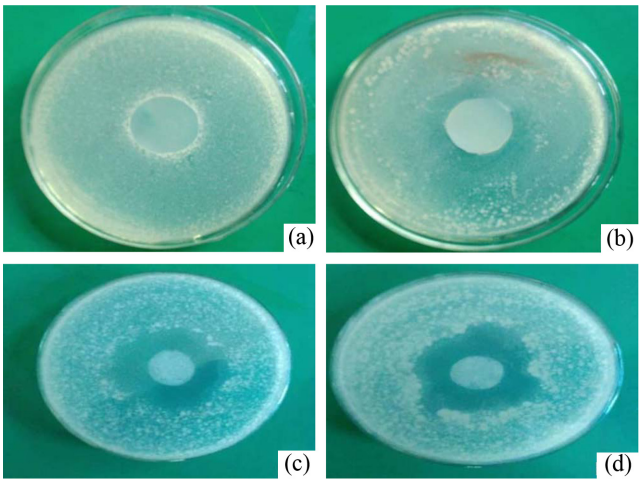

Figure 8. Antibacterial properties image of *Escherichia coli* of PLA based nanocomposites: (a) P0; (b) PTZ5; (c) PTZ9; (d) PTZ15.

the calculated areas of bacteriostatic rings of PLA based nanocomposites, which increased with the addition of ZnO pillared organic saponite. The areas of bacteriostatic rings of *Bacillus subtilis* and *Escherichia coli* were increased by 2.72 times and 3.01 times compared to that of the control sample, respectively. The reason could be that the reactive oxygen was produced by the excitation of nano ZnO probably combined with the cellular matter of bacteria, thereby killing them.[28]

Conclusions

A series of novel PLA/ZnO pillared organic saponite nanocomposites were successfully prepared by a solution intercalation method in order to improve the crystallization and functional performance of PLA materials. Here, ZnO pillared organic saponite was stripped into nanoscale layers. This induced a heterogeneous nucleation effect in PLA matrix, which accelerated the crystallization of PLA. In addition, it was experimentally shown that ZnO pillared organic saponite enhanced the mechanical performance and thermal stability of PLA based nanocopmposites, which was also a novelty. Above all, this nanocomposite not only showed absorption peaks in the ultraviolet wavelength region, but also inhibited the bacterial growth by forming a ring around it. Furthermore, the antibacterial properties were increased with the addition of ZnO pillared organic saponite.

Acknowledgement: Financial support from National Science Foundation of China (51163013) is greatly acknowledged.

References

1. S. Y. Nan, Z. Y. Fang, and Z. W. Jun, *Polym. Korea*, **39**, 261 (2015).
2. Q. Zhou and M. Xanthos, *Polym. Degrad. Stab.*, **94**, 327 (2009).
3. J. E. Jang, H. Y. Kim, J. E. Song, D. Lee, S. Y. Kwon, J. W. Chung, and G. Khang, *Polym. Korea*, **37**, 669 (2013).
4. J. H. Cha, S. J. Ahn, and H. Y. Jeon, *Polym. Korea*, **39**, 566 (2015).
5. J. Y. Nam, M. Okamoto, H. Okamoto, M. Nakano, A. Usuki, and M. Matsuda, *Polymer*, **47**, 1340 (2006).
6. W. J. Zhen and J. L. Sun, *Polym. Korea*, **38**, 299 (2013).
7. S. H. Lee, D. Kim, J. H. Kim, D. H. Lee, S. J. Sim, J. D. Nam, H. Kye, and Y. K. Lee, *Polym. Korea*, **28**, 519 (2004).
8. J. R. Lee, S. W. Chun, and H. J. Kang, *Polym. Korea*, **27**, 285 (2003).
9. X. Xi, W. J. Zhen, S. Z. Bian, and W. T. Wang, *Polym. Korea*, **39**, 601 (2015).
10. M. Farhoodi, S. Dadashi, S. M. A. Mousavi, R. Sotudeh-Gharebagh, Z. Emam-Djomeh, A. Oromiehie, and F. Hemmati, *Polym. Korea*, **36**, 745 (2012).
11. M. A. Paul, M. Alexandre, P. Degée, C. Henrist, A. Rulmont, and P. Dubois, *Polymer*, **44**, 443 (2003).
12. W. Zhen, C. Lu, C. Li, and M. Liang, *Appl. Clay Sci.*, **57**, 64 (2012).
13. M. Kitano, T. Hamabe, and S. Maeda, *J. Cryst. Growth*, **102**, 965 (1990).
14. K. Ogata, K. Maejima, S. Fujita, and S. Fujita, *J. Cryst. Growth*, **248**, 25 (2003).
15. P. Fons, K. Iwata, A. Yamada, K. Matsubara, S. Niki, K. Nakahara, T. Tanabe, and H. Takasu, *Appl. Phys. Lett.*, **77**, 1801 (2000).
16. J. Li and W. Zhen, *Acta Polym. Sinica*, **4**, 534 (2013).
17. W. T. Wang, W. J. Zhen, S. Z. Bian, and X. Xi, *Appl. Clay Sci.*, **109**, 136 (2015).
18. Z. Gui, C. Lu, and S. Cheng, *Polym. Test.*, **32**, 15 (2013).
19. Z. Tang, C. Zhang, X. Liu, and J. Zhu, *J. Appl. Polym. Sci.*, **125**, 1108 (2012).
20. S. Lee, H. Park, H. Lim, T. Kang, X. Li, W. Cho, and C. Ha, *Polymer*, **43**, 2495 (2002).
21. B. Li, F. Dong, X. Wang, J. Yang, D. Wang, and Y. Wang, *Eur. Polym. J.*, **45**, 2996 (2009).
22. D. Y. Zuo, L. Zhang, and C. H. Yi, *Polym. Adv. Technol.*, **25**, 1406 (2014).
23. A. Mathew, K. Oksman, and M. Sain, *J. Appl. Polym. Sci.*, **101**, 300 (2006).
24. K. Mogyorósi, J. Németh, I. Dékány, and J. Fendler, *Prog. Colloid Polym. Sci.*, **117**, 88 (2002).
25. S. Bourbigot, G. Fontaine, and A. Gallos, *Polym. Adv. Technol.*, **22**, 30 (2011).
26. H. Bai, H. Xiu, J. Gao, H. Deng, Q. Zhang, M. Yang, and Q. Fu, *ACS Appl. Mater. Inter.*, **4**, 897 (2012).
27. W. J. Jeong, S. K. Kim, and G. C. Park, *Thin Solid Films*, **506**, 180 (2006).
28. N. Jones, B. Ray, K. Ranjit, and A. Manna, *FEMS Microbiol. Lett.*, **79**, 71 (2008).